ISSN 1990-7931, Russian Journal of Physical Chemistry B, 2024, Vol. 18, No. 1, pp. 49–66. © Pleiades Publishing, Ltd., 2024.

STRUCTURE OF CHEMICAL COMPOUNDS, QUANTUM CHEMISTRY, SPECTROSCOPY

In Situ Ti-Embedded SiC as Chemiresistive Nanosensor for Safety Monitoring of CO, CO_2, NO, NO_2: Molecular Modelling by Conceptual Density Functional Theory

F. Mollaamin[a, b, *] and M. Monajjemi[c]

[a] *Department of Food Engineering, Faculty of Engineering and Architecture, Kastamonu University, Kastamonu, Turkey*
[b] *Department of Biology, Faculty of Science, Kastamonu University, Kastamonu, Turkey*
[c] *Department of Chemical Engineering, Central Tehran Branch, Islamic Azad University, Tehran, Iran*
**e-mail: smollaamin@gmail.com*

Received June 14, 2023; revised July 21, 2023; accepted September 20, 2023

Abstract—The adsorption of four CO, CO_2, NO, NO_2 gas molecules in the atmosphere on titanium (Ti)-doped monolayer SiC surface was investigated using the density functional theory (DFT) with equilibrium geometries optimized at the CAM-B3LYP/6-311+G(*d*, *p*) level of theory. The thermochemical, electric and magnetic properties data recommend that the adsorption of these gas molecules on Ti-embedded SiC sheet (SiC_sh) monolayer is more energetically desired than that on the pristine ones. Gas molecules of CO, CO_2, NO, NO_2 have been adsorbed on the Ti site of doped SiC monolayer through the formation of covalent bonds. Moreover, after the adsorption, the orientations of the gas molecules exhibited a tendency to orient in the inclined and parallel forms to monolayer SiC_sh. The DFT analysis explored that the monolayer SiC_sh with C and Ti-doped atoms possessing one satisfied valency increased the Van der Waal interactions between the gas molecules and the monolayer SiC_sh. Furthermore, the assumption of chemical adsorptions has been approved by the projected density of states (PDOS) and charge density difference plots. Charge density difference calculations also indicate that the electronic densities were mainly accumulated on the adsorbate of CO, CO_2, NO, NO_2 gas molecules. The results in this investigation can indicate the competence of transition metal doped silicon carbide nanosheet in sensor devices. The overall analysis showed that the adsorption strength of monolayer SiC_sh towards the chosen gas molecules follows the order: $NO_2 > CO_2 > NO > CO$.

Keywords: gas sensor, Ti–SiC_sh, CO, CO_2, NO, NO_2, DFT
DOI: 10.1134/S1990793124010159

INTRODUCTION

Graphene with two-dimensional (2D) layered physical structure and the unique electronic properties has simulated a broad range of research enthusiasm on 2D materials which can be applied for the electronic, optoelectronic, and spintronic devices [1–11].

But, the practical application of 2D material like graphene might be confined with small band gap. Thus, new 2D materials with perfect mechanical, thermoelectric, optical and electronic properties are the clue to the recent scientific investigations [12–15].

In transition metal (TM) decorated carbon nanostructure, the TM-carbon binding takes place through a charge-transfer mechanism and the TM remains in the cationic state. Therefore, the gas molecule can get absorbed on the cationic transition metal element giving some electronic charge [16–19].

The Silicon Carbide (SiC) monolayer as a new graphene-like semiconductor is a direct band gap material, while silicon being in the same group with the carbon represents attributes entirely analogous to that of carbon and makes it possible to generate powerful applications in optoelectronic and electronic instruments [20–25]. As the polarizability of Si is more than C, so it is expected that, due to stronger van der Waal's interaction, SiC/Si nanosurface can bind compounds more strongly compared to the pure carbon nanostructures. It is known that for optimum adsorption of gas molecules, the ideal form of binding between the host material (SiC nanosheet) and adsorbed gas molecules should be intermediate between physisorption and chemisorption energy [26].

In addition, transition metal (TM) atoms are considered to be the source of magnetism; in the results of TM-doped SiC monolayer, it can be found that the system can be a magnetic semiconductor by Co, Cu, Fe, Mn, and Ni doping [27]. The TM dopants can cause a total Hamiltonian perturbation, eventually leading to changes in electronic structures, which makes it a substantial application in magnetic electronic devices [28–34].

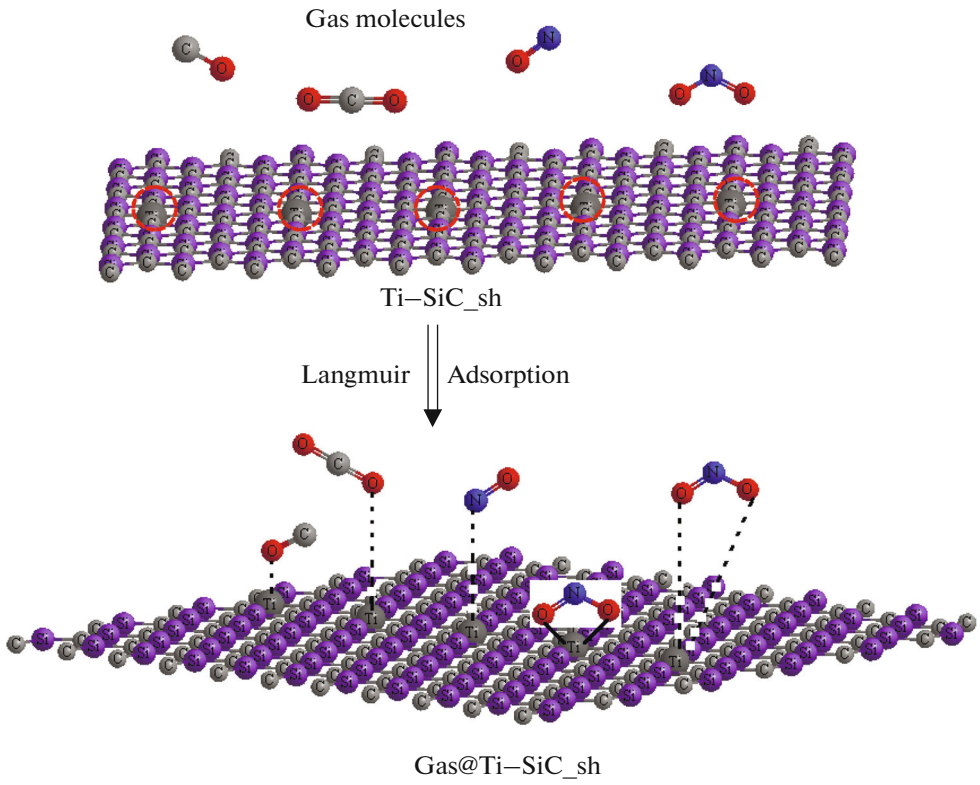

Fig. 1. Langmuir adsorption of CO, CO_2, NO, and NO_2 onto Ti-doped SiC nanosheet.

In this work, we shall present the theoretical estimates for the charge transfer and the energy of binding with the SiC surface for adsorption of molecules. Then, it has been investigated the magnetic and electronic structures of Ti-doped graphene-like SiC sheet through adsorption of CO, CO_2, NO, NO_2 gas molecules (GM@Ti–SiC_sh) by using first-principle calculations based on the density functional theory (DFT) [35]. The calculation is realized by generalized gradient approximation (GGA) potential and Perdew–Burke–Ernzerhof (PBE) functional [36, 37].

MATERIALS AND METHOD

In this article, the SiC graphene-like sheet has been modeled It was prepared by chirality ($n = 10$, $m = 0$), surface length (25 Å), bond length (1.421 Å), and MWNT (1, 2, 0), and then minimized by alternatively arranged 15 C and 15 Si atoms. In a previous theoretical calculation it is reported that the most stable structure of planar SiC forms graphene-like structure with alternative SiC bond and the bonding in such structure is of sp^2 type (Fig. 1) [38]. In our calculation we have considered similar structure and optimized without any symmetry constraint.

The adsorbing of CO, CO_2, NO, NO_2 gas molecules on the surface of Ti–SiC_sh was defined by the theory Langmuir isotherm [39, 40], which indicates the chemisorption between gas molecules and Ti–SiC_sh. The adsorbates of CO, CO_2, NO, NO_2 gas molecules are maintained on surface of Ti–SiC_sh with "Langmuir" chemisorption (Fig. 1).

In this research, the simulated calculations have been directed in the GaussView 6.06.16 [41] and calculated by Gaussian 16, Revision C.01 [42] using the DFT method. The Perdew–Burke–Ernzerhof (PBE) functional with high-precision generalized gradient approximation (GGA) has been employed to achieve more authentic results [36].

The electronic, magnetic, and optical behaviors of adsorption of gas molecules on the Ti-doped SiC_sh have been measures. The binding energy is calculated as: $E_b = (E_t - 15E_{Si} - 15E_C)/30$, where E_t is the total energy after optimization, E_{Si} and E_C are the correction factors for Si and C atoms, respectively. The binding energy results show that all the gas molecules (GM)-adsorbed SiC systems are stable.

From the charge density distribution of the SiC sheet, it is seen that a considerable amount of electronic charge is transferred from Si to C site. The presence of these point charges on the SiC sheet influences the gas adsorption property.

After organizing the structure and energetics of SiC sheet, we have tried to decorate the sheet by titanium atom. A full geometry optimization has been done and the data has explored that the most stable location of

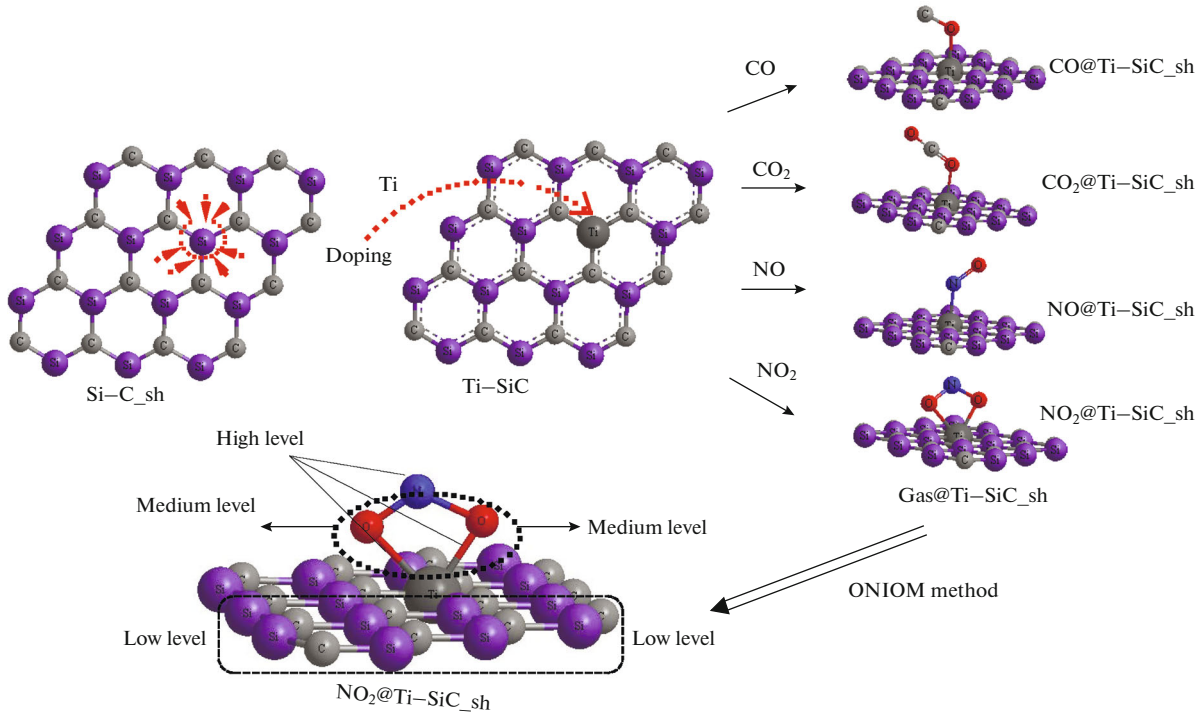

Fig. 2. The ONIOM method through adsorption of CO, CO_2, NO, and NO_2 gas molecules onto Ti-doped SiC nanosheet based on optimized coordination due to three-layered of high, medium and low levels of ONIOM method.

titanium is on the top of Si atom by pushing it down the surface.

Figure 2 has shown that the SiC sheet is distorted from planarity after adding the titanium in such a way that the doped titanium can bind with Si atom along with three neighboring carbon atoms, therefore developing the stability of the system. When the titanium atom is on the silicon atom, the Ti–Si bond distance is 2.56 Å while Ti–C bond distance is 1.98 Å. After doping of titanium on the silicon atom, the planarity of the system is perturbed because silicon atom goes toward the sp^3 hybridization. Although silicon and carbon atoms are iso-valent, the most stable state of carbon is sp^2 and silicon is sp^3. Then, we have tailored the spin-polarized DFT calculation with Our own N-layered Integrated molecular Orbital and Molecular mechanics (ONIOM) model [43, 44] accompanying the same force and energy convergence accuracy to the adsorption systems, with CAM-B3LYP functional and with 6-311+G (*d*, *p*) [45] basis set for carbon, nitrogen, oxygen, silicon and LANL2DZ for titanium in the adsorption sites for the first layer (high level). Second layer (medium level) has been considered on some titanium atoms, carbon, and silicon atoms of SiC_sh, respectively, in the adsorption site due to semi-empirical methods. The third layer (low level) has been saved on the remained carbon and silicon atoms of SiC_sh with molecular mechanic force fields (Fig. 2) [44] as formula:

$$E_{\mathrm{ONION}} = E_{1\mathrm{st}} + E_{2\mathrm{nd}} + E_{3\mathrm{rd}}. \quad (1)$$

It has been studied the interaction of CO, CO_2, NO, and NO_2 gas molecules with the Ti decorated SiC sheet. The optimized geometries of the GM@Ti decorated SiC sheet are shown in Fig. 2.

The charge transfer between adsorbates of CO, CO_2, NO, NO_2 and adsorbent of Ti–SiC_sh is calculated due to the Bader charge analysis [46]. This method can measure charge accumulation from the charge of each atom in the complex model. Finally, the total adsorption charge transfer can be obtained as formula:

$$\Delta Q_t = Q_2 - Q_1,$$

where Q_2 and Q_1 remark the charge of CO, CO_2, NO, NO_2 after and before adoption, respectively. In fact, negative ΔQ_t indicates that electrons are transferred from gas molecules of CO, CO_2, NO, NO_2 to the surface of Ti–SiC_sh, and the adsorbent acts as an electron acceptor [47, 48].

The changes of charge density analysis in the adsorption process has illustrated that Ti–SiC_sh shows the Bader charge of $-1.307e$, before adsorption of CO,CO_2, NO, NO_2, and $-1.309e$, $-1.301e$, $-1.330e$, $-1.348e$ after adsorption of CO,CO_2, NO, NO_2, respectively. Therefore, the changes of charge density for Langmuir adsorption of CO, CO_2, NO,

NO_2 on Ti–SiC_sh surface alternatively are $\Delta Q_{CO_2\to Ti-SiC} = +0.006e > \Delta Q_{CO\to Ti-SiC} = +0.002e > \Delta Q_{NO\to Ti-SiC} = -0.023e > \Delta Q_{NO_2\to Ti-SiC} = -0.041e$. The values of changes of charge density have shown a more important charge transfer for Ti–SiC_sh which acts as the electron acceptor while gas molecules of NO_2 and NO act as the stronger electron donors through adsorption on the Ti–SiC_sh surface.

To determine the most sensitive structure of Ti–SiC_sh as the selective sensor for detecting gas molecules of CO, CO_2, NO, and NO_2, the binding energy of each system has been calculated. Therefore, we have found that the priority for selecting the surface binding of N-atom of NO, and O-atom of NO_2, CO, CO_2, in adsorption site can be impacted by the existence of close atoms in the Ti–SiC_sh surface. The simulated distribution functions of NO → Ti–SiC_sh, NO_2 → Ti–SiC_sh, CO → Ti–SiC_sh, and CO_2 → Ti–SiC_sh have illustrated that the created clusters lead to the bond lengths of N →Ti in NO → Ti–SiC_sh (2.07 Å), O →Ti in NO_2 → Ti–SiC_sh (2.06 Å), O → Ti in CO → Ti–SiC_sh (2.05 Å) and O → Ti in CO_2 → Ti–SiC_sh (2.05 Å) (Figs. 1, 2).

Furthermore, the nuclear quadrupole resonance (NQR) procedure has been carried out for the complexes of gas molecules of CO, CO_2, NO and NO_2 adsorbing on Ti–SiC_sh. NQR is related to the multipole enlargement in cartesian harmonies as follows [49, 50]:

$$V(r) = V(0) + \left[\left(\frac{\partial V}{\partial x_i}\right)_0 x_i\right] + \frac{1}{2}\left[\left(\frac{\partial^2 V}{\partial x_i x_j}\right)_0 x_i x_j\right] + \ldots, \quad (2)$$

$$U = -\frac{1}{2}\int_{\mathcal{D}} d^3 r \rho_r \left[\left(\frac{\partial^2 V}{\partial x_i^2}\right)_0 x_i^2\right] = -\frac{1}{2}\int_{\mathcal{D}} d^3 r \rho_r \left[\left(\frac{\partial E_i}{\partial x_i}\right)_0 x_i^2\right] = -\frac{1}{2}\left(\frac{\partial E_i}{\partial x_i}\right)_0 \int_{\mathcal{D}} d^3 r \left[\rho(r) x_i^2\right]. \quad (3)$$

There are two factors which should be gotten from nuclear quadrupole resonance experiments; the quadrupole coupling constant, χ, and asymmetry factor of the electric field gradient tensor η:

$$\chi = e^2 Q q_{zz}/h, \quad (4)$$

$$\eta = q_{xx} - q_{yy}/q_{zz}, \quad (5)$$

while q_{ii} are ingredients of the electric field gradient tensor at the quadrupole nucleus assigned in the electric field gradient principal axes system, e—the proton charge and h is the Planck's constant and Q the nuclear quadrupole moment [51, 52].

RESULTS AND DISCUSSION

In this verdict, titanium (Ti) metal-doped graphene-like silicon carbide (SiC) monolayer sheet has been investigated as the efficient surface because of their structural selectivity for adsorption of carbon monoxide (CO), carbon dioxide (CO_2), nitric oxide (NO), and nitrogen dioxide (NO_2). These experiments have been accomplished using spectroscopy analysis through some physical and chemical properties.

The electronic structures of gas molecules (GM) of CO, CO_2, NO and NO_2 adsorbed on the Ti-doped SiC nanosheet (GM@Ti–SiC_sh) have been analyzed to simplify subsequent discussion for interfacial electronic properties. Figure 3 shows the projected density of state (PDOS) of the Ti decorated SiC sheet. The appearance of the energy states (*d*-orbital) of Ti within the gap of SiC sheet induces the reactivity of the system. It is clear from the figure that after doping with Ti atom and there is a significant contribution of Ti *d*-orbital in the unoccupied level. Based on the population analysis and DOS it can be concluded that Ti remains in the cationic state and it can accept more electrons from other atoms. Therefore, the graph of partial DOS (PDOS) has illustrated that the *p* states of the adsorption of N- and O- on the Ti–SiC_sh are dominant through the conduction band (Fig. 3). A distinct metallic feature can be observed in SiC_sh because of the strong interaction between the *p* states of C, N, O, Si and the *d* state of Ti near the Fermi energy. Moreover, the existence of covalent features for these complexes has exhibited the identical energy amount and figure of the PDOS for the *p* orbitals of C, N, O, Si and *d* orbitals of Ti (Figs. 3a–3d and 3a'–3d').

Figures 3a, 3a' and 3b, 3b' shows that the CO and CO_2 states, respectively, onto SiC_sh and Ti–SiC_sh, respectively, have more contribution at the middle of the conduction band between −5 to −10 eV, while contribution of carbon and silicon sates are expanded and close together, but titanium states have minor contributions and silicon have major contributions in SiC_sh.

Figures 3c, 3c' and 3d, 3d' shows that the NO and NO_2 states, respectively, onto SiC_sh and Ti–SiC_sh, respectively, have more contribution at the middle of the conduction band between −5 to −10 eV, while contribution of carbon and silicon sates are expanded and close together, but titanium states have major contributions in Ti–SiC_sh and silicon have major contributions in SiC_sh.

The results also approved by the partial electron density (PDOS) which have showed a certain charge association between Ti–SiC_sh and gas molecules of CO, CO_2, NO and NO_2.

Therefore, the above results exhibit that the cluster dominant of non-metallic and metallic features and a certain degree of covalent features can illustrate the increasing of the semiconducting direct band gap of

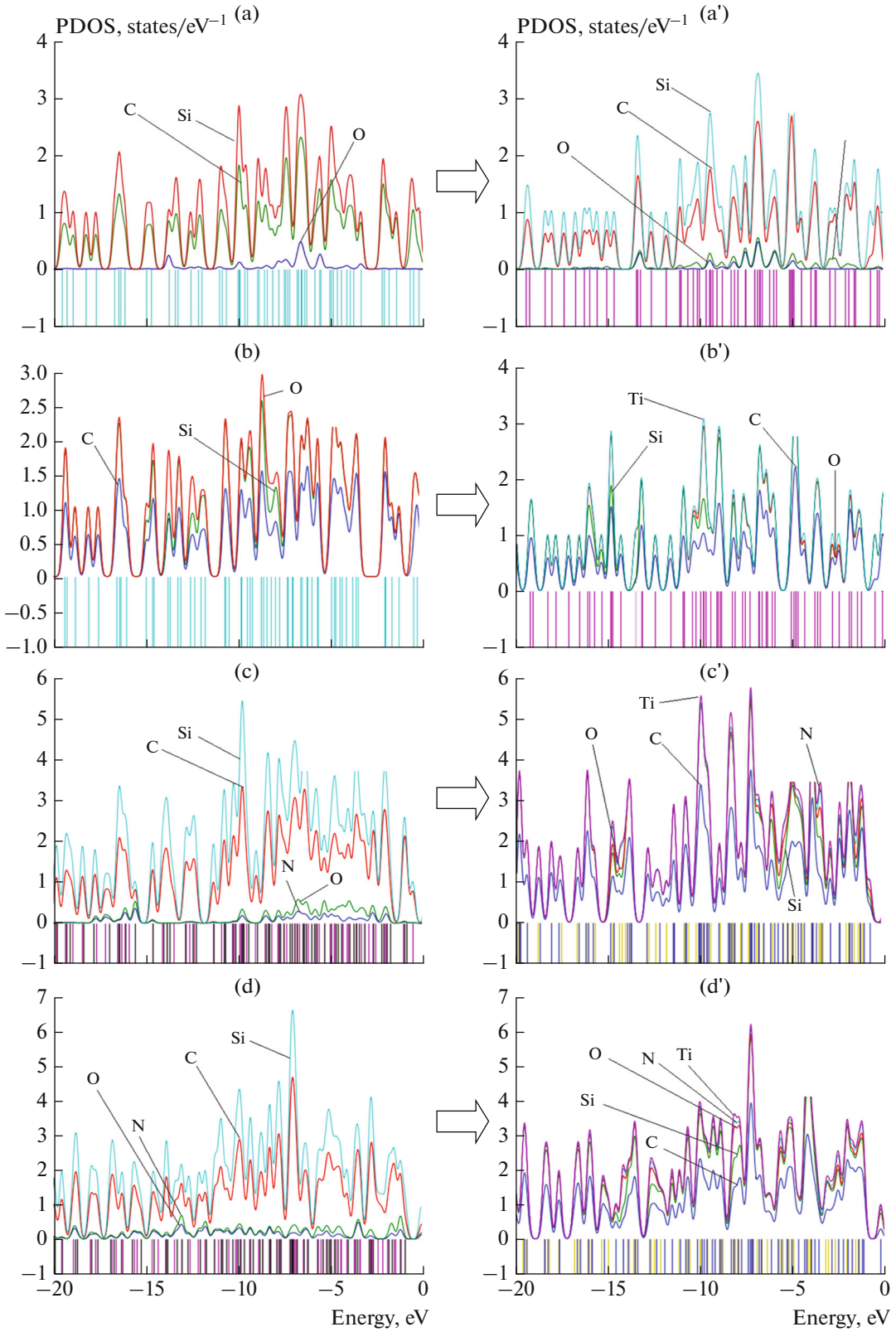

Fig. 3. PDOS adsorption of (a) CO@SiC_sh, (a') CO@Ti–SiC_sh, (b) CO_2@SiC, (b') CO_2@Ti–SiC, (c) NO@SiC, (c') NO@Ti–SiC, (d) NO_2@SiC, and (d') NO_2@Ti–SiC.

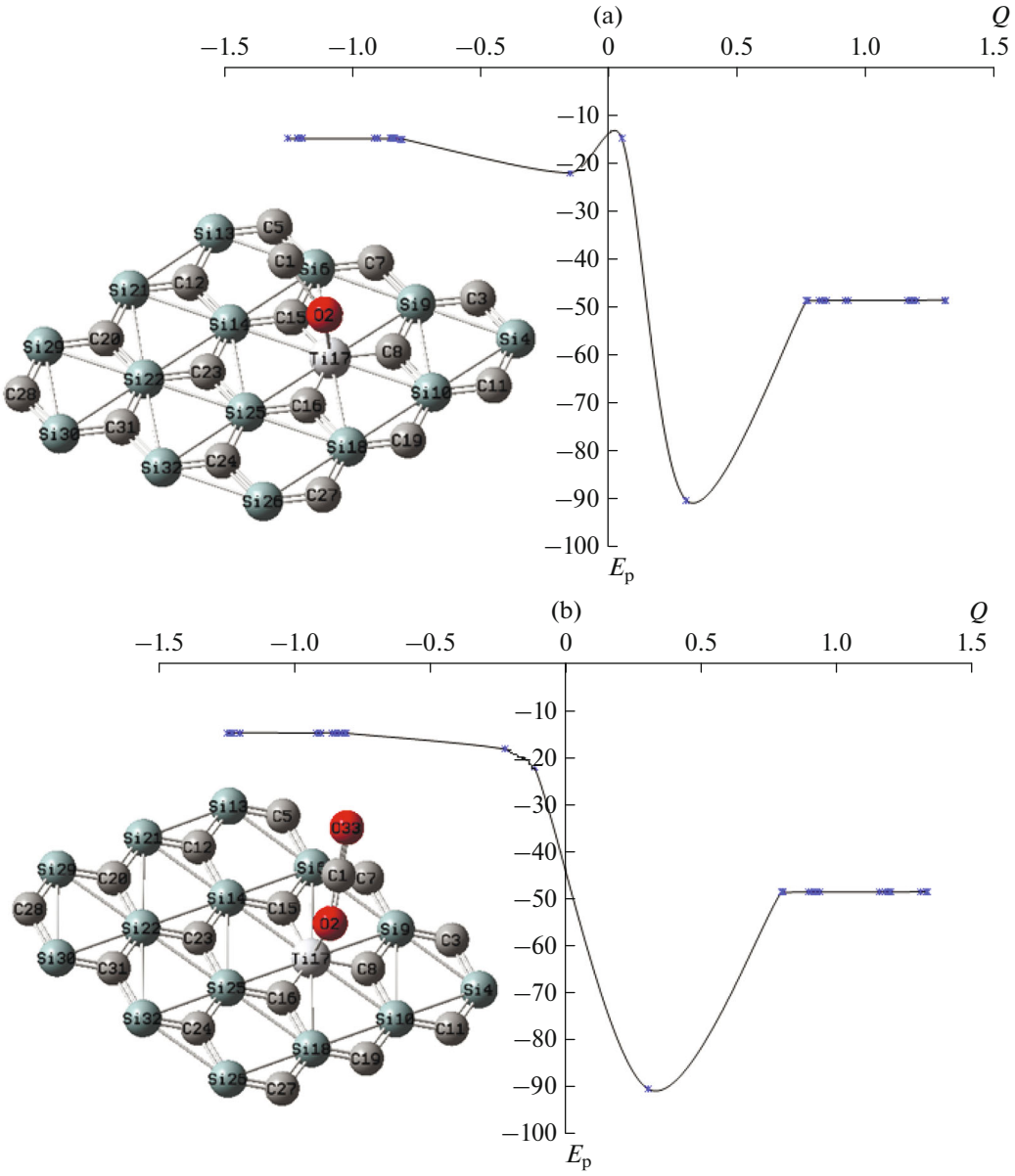

Fig. 4. The electric potential versus Bader charge through NQR calculation for adsorption clusters of (a) CO@Ti–SiC_sh, (b) CO_2@Ti–SiC_sh, (c) NO@Ti–SiC_sh and (d) NO_2@Ti–SiC_sh by using CAM-B3LYP/EPR-III, LANL2DZ,6-31+G(*d*, *p*).

gas molecules of CO, CO_2, NO and NO_2 adsorbing on Ti–SiC_sh.

Since the electric field gradient at the situation of NO and NO_2 adsorbed on the Ti–SiC_sh surface as the gas detector is approved by the valence electrons distorted in the special connection with close nuclei of Ti-doped SiC nanosheet, the nuclear quadrupole resonance (NQR) at which transitions occur is special for CO@Ti–SiC_sh, CO_2@Ti–SiC_sh, NO@Ti–SiC_sh and NO_2@Ti–SiC_sh (Table 1).

Furthermore, in Figs. 4a–4d, it has been drawn the electric potential of nuclear quadrupole resonance method versus Bader charge for elements of carbon, nitrogen, oxygen, silicon and titanium in the adsorption process of CO, CO_2, NO and NO_2 on the Ti-doped SiC nanosheet by CAM-B3LYP/EPR-III, 6-311+G(*d*, *p*), LANL2DZ theoretical level.

In Figs. 4a–4d, it has been remarked the changes of electric potential for carbon, nitrogen, oxygen, silicon and titanium in the active site of Langmuir adsorption. In fact, it has been observed the effect of the binding between C, N and O atoms of gas molecules with titanium doping in the SiC nanosheet during adsorbing CO, CO_2, NO and NO_2 through resulted electric potential using NQR analysis (Figs. 4a–4d). It's obvious that the capability of SiC nanosheet for detecting

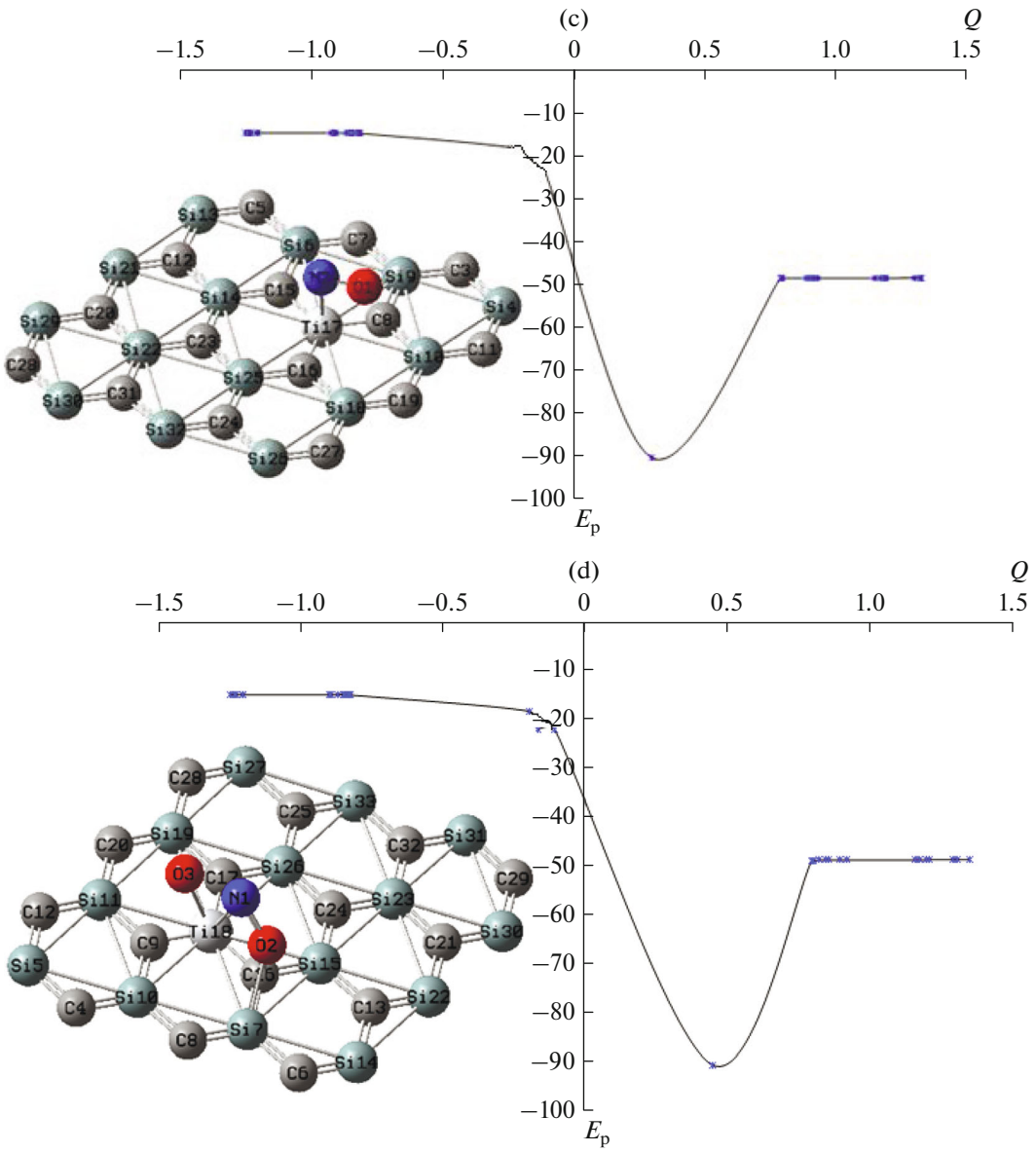

Fig. 4. (Contd.)

of CO, CO_2, NO and NO_2 is fluctuated by their selectivity and sensitivity which can represent the efficiency of these surfaces as the promising sensors.

Isotropic (σ_{iso}/ppm) and anisotropy (σ_{aniso}/ppm) shielding tensors of NMR spectroscopy [53] for certain atoms in the active site of CO, CO_2, NO and NO_2 adsorbed on the Ti-doped SiC nanosheet (GM@Ti–SiC_sh) (Figs. 4a–4d) through the formation of the binding between gas molecules and solid surfaces have been calculated using Gaussian 16, Revision C.01 and reported in Table 2 [42].

It was observed the chemical shielding (ppm) of "NMR" curves versus atom type through adsorption of CO, CO_2, NO and NO_2 adsorbed on the Ti–SiC nanosheet (Figs. 5a–5d).

The resulted graphs of NMR data in Figs. 5a–5d have shown approximately the identical chemical shielding behavior of isotropic and anisotropy factors of GM @Ti–SiC_sh with several sharp peaks related to carbon, nitrogen, oxygen, silicon and titanium of gas molecules (adsorbate) and TM-doped SiC nanosheet (adsorbent) in the active site situations (Figs. 5a–5d. CO@Ti–SiC_sh with several sharp peaks related to the adsorption site for atoms including C1, C7, C11, C19, C28, Si4, Si21, Si29, Si30, Ti17 (Fig. 5a); CO_2@Ti–SiC_sh with several sharp peaks for atoms of C7, C11, C19, C28, Si13, Si21, Si29, Si30,Ti17 (Fig. 5b); NO@Ti–SiC_sh with several sharp peaks for atoms of O1, N2, Ti17 and several less sharped peaks for atoms of C5, C8, C28, Si13, Si26

Table 1. The electric potential (E_p) and Bader charge (Q) for elements involving in the adsorption mechanism of CO, CO_2, NO and NO_2 adsorbed on the Ti-doped SiC nanosheet using CAM-B3LYP/EPR-III, 6-311+G(d, p) calculation extracted of NQR method

CO@Ti–SiC_sh			CO_2@Ti–SiC_sh			NO@Ti–SiC_sh			NO_2@Ti–SiC_sh		
Atom	Q	E_p	Atom	Q	E_p	Atom	Q	E_p	Atom	Q	E_p
C1	0.0447	−14.6763	C1	0.4328	−14.2805	O1	−0.1160	−22.0984	N1	−0.1969	−18.1387
O2	−0.1564	−21.9577	O2	−0.1395	−21.7704	N2	−0.2251	−18.2494	O2	−0.1637	−21.8078
C3	−0.8532	−14.8484	C3	−0.8442	−14.8355	C3	−0.8495	−14.8598	O3	−0.1053	−21.9782
Si4	0.8155	−48.6319	Si4	0.7909	−48.6507	Si4	0.7918	−48.6641	C4	−0.8396	−14.8468
C5	−0.8425	−14.8444	C5	−0.8435	−14.8587	C5	−0.8121	−14.8302	Si5	0.7957	−48.6525
Si6	1.1614	−48.5789	Si6	1.1362	−48.5859	Si6	1.1551	−48.5961	C6	−0.8281	−14.8278
C7	−0.8115	−14.8673	C7	−0.8343	−14.8872	C7	−0.8372	−14.9081	Si7	1.2098	−48.5438
C8	−0.9190	−14.825	C8	−0.9272	−14.8388	C8	−0.9186	−14.8321	C8	−0.8263	−14.8809
Si9	1.1768	−48.5713	Si9	1.1635	−48.5892	Si9	1.1942	−48.5956	C9	−0.8940	−14.817
Si10	1.1928	−48.5739	Si10	1.1602	−48.5836	Si10	1.1906	−48.5954	Si10	1.1599	−48.5914
C11	−0.8404	−14.8227	C11	−0.8625	−14.8692	C11	−0.8506	−14.8624	Si11	1.1976	−48.5827
C12	−1.2017	−14.8138	C12	−1.2018	−14.8207	C12	−1.1988	−14.785	C12	−0.8404	−14.8465
Si13	0.8416	−48.631	Si13	0.8125	−48.6483	Si13	0.8008	−48.6357	C13	−1.2007	−14.7818
Si14	1.3083	−48.516	Si14	1.2855	−48.5247	Si14	1.3238	−48.5129	Si14	0.8212	−48.6232
C15	−0.9057	−14.8229	C15	−0.9268	−14.8323	C15	−0.9015	−14.8175	Si15	1.3475	−48.4816
C16	−0.9042	−14.8213	C16	−0.9097	−14.8292	C16	−0.9025	−14.8232	C16	−0.8481	−14.6962
Ti17	0.2976	−90.3994	Ti17	0.3264	−90.4046	Ti17	0.3051	−90.4117	C17	−0.8887	−14.8371
Si18	1.1764	−48.5753	Si18	1.1497	−48.5896	Si18	1.1735	−48.5843	Ti18	0.4458	−90.3755
C19	−0.8170	−14.867	C19	−0.8188	−14.8821	C19	−0.8089	−14.878	Si19	1.1721	−48.5887
C20	−1.2182	−14.7736	C20	−1.2182	−14.7838	C20	−1.2280	−14.7708	C20	−0.8312	−14.8991
Si21	0.7656	−48.6669	Si21	0.7517	−48.6802	Si21	0.9043	−48.5752	C21	−1.2257	−14.7855
Si22	1.3086	−48.5091	Si22	1.3007	−48.517	Si22	1.3049	−48.503	Si22	0.8444	−48.6149
C23	−1.2538	−14.8339	C23	−1.2555	−14.8391	C23	−1.2485	−14.8287	Si23	1.3041	−48.5097
C24	−1.2008	−14.8144	C24	−1.2022	−14.8193	C24	−1.1983	−14.7793	C24	−1.2465	−14.8154
Si25	1.3080	−48.5195	Si25	1.2971	−48.5228	Si25	1.3301	−48.5044	C25	−1.1999	−14.785
Si26	0.8269	−48.6394	Si26	0.8321	−48.6372	Si26	0.7966	−48.6375	Si26	1.2913	−48.5139
C27	−0.8427	−14.851	C27	−0.8438	−14.8489	C27	−0.8223	−14.8369	Si27	0.8008	−48.6358
C28	−0.8525	−14.7777	C28	−0.8560	−14.7903	C28	−0.8603	−14.7703	C28	−0.8240	−14.8373
Si29	0.9254	−48.5726	Si29	0.9042	−48.5918	Si29	0.9173	−48.5441	C29	−0.8675	−14.8003
Si30	0.9194	−48.5762	Si30	0.9135	−48.5849	Si30	0.8903	−48.5625	Si30	0.8935	−48.5776
C31	−1.2184	−14.7745	C31	−1.2179	−14.7822	C31	−1.2329	−14.7826	Si31	0.8545	−48.5954
Si32	0.7691	−48.6662	Si32	0.7483	−48.6786	Si32	0.9327	−48.5653	C32	−1.2315	−14.7995
			O33	−0.1036	−21.7854				Si33	0.9200	−48.579

Table 2. Data of gauge including atomic orbital (GIAO)/nuclear magnetic resonance (NMR) shielding tensors/ppm for selected atoms of CO, CO_2, NO and NO_2 adsorbed on the Ti-doped SiC nanosheet (GM@Ti–SiC_sh) using CAM-B3LYP/EPR-III, 6-311+G(*d*, *p*) calculation

CO@Ti–SiC_sh			CO_2@Ti–SiC_sh			NO@Ti–SiC_sh			NO_2@Ti–SiC_sh		
Atom	σ_{iso}, ppm	σ_{aniso}, ppm	Atom	σ_{iso}, ppm	σ_{aniso}, ppm	Atom	σ_{iso}, ppm	σ_{aniso}, ppm	Atom	σ_{iso}, ppm	σ_{aniso}, ppm
C1	11111.4472	24988.0432	C1	145.4006	210.9101	O1	2336.2195	2980.2105	N1	65.1036	342.5979
O2	2479.6300	5187.8214	O2	299.6111	162.9497	N2	805.0526	1027.1995	O2	235.4150	158.3215
C3	907.6908	2420.3768	C3	425.5927	1178.2736	C3	60.1550	315.5590	O3	141.4255	1217.9976
Si4	2088.0883	5367.7686	Si4	99.7387	972.5214	Si4	423.5479	333.0246	C4	76.0664	247.2353
C5	74.4146	412.2807	C5	81.6083	514.4560	C5	63.3853	473.6899	Si5	388.3425	406.7643
Si6	878.0865	1854.4291	Si6	538.7382	402.3132	Si6	547.1460	205.2232	C6	81.5389	511.2567
C7	2715.9557	11547.4885	C7	1311.6230	2196.3916	C7	44.5324	166.3661	Si7	569.9207	198.6516
C8	1488.6353	3719.2313	C8	532.4831	967.7295	C8	15.1484	506.9911	C8	31.5175	182.2533
Si9	520.3949	558.6553	Si9	531.8902	308.3004	Si9	548.1179	180.5936	C9	152.4698	166.3381
Si10	427.4353	538.1887	Si10	487.2460	286.5483	Si10	498.9470	181.7101	Si10	503.5350	189.7524
C11	694.0893	4169.9333	C11	100.8839	899.6612	C11	125.0332	225.3520	Si11	493.1364	180.3917
C12	528.5808	995.4705	C12	184.0750	154.0651	C12	222.1382	60.0991	C12	95.9930	249.4879
Si13	109.4815	1142.8126	Si13	372.8765	679.4168	Si13	312.1764	666.1447	C13	250.0360	167.7335
Si14	812.7671	1834.8867	Si14	470.0050	470.0050	Si14	488.9875	112.7812	Si14	201.5410	943.1709
C15	390.8768	2337.0998	C15	279.4190	225.3213	C15	81.7264	242.3315	Si15	440.5262	230.2631
C16	324.1900	1766.0828	C16	267.3022	392.7469	C16	12.5167	393.1278	C16	110.0590	160.4944
Ti17	4441.5114	12062.8971	Ti17	0.2898	2319.4610	Ti17	2193.9940	2915.8766	C17	152.9803	121.2933
Si18	684.7339	453.4367	Si18	470.7647	362.8494	Si18	534.7415	226.7653	Ti18	486.5292	524.9393
C19	3713.7019	13466.0765	C19	986.2897	1699.6083	C19	43.8868	308.6632	Si19	489.9162	203.0216
C20	3310.0396	5480.1033	C20	405.8085	542.9896	C20	141.5596	145.6224	C20	22.7374	179.8416
Si21	2703.7518	8957.9647	Si21	159.6671	1012.0255	Si21	253.2383	205.2387	C21	30.6631	306.4868
Si22	976.7021	1668.0964	Si22	480.8095	208.0491	Si22	395.1189	187.6411	Si22	413.6272	1393.2065
C23	390.9605	743.8175	C23	235.0254	155.6737	C23	220.3842	94.5052	Si23	547.1171	299.1860
C24	25.5229	422.1970	C24	105.0097	268.4400	C24	198.8207	112.7170	C24	243.0867	158.9151
Si25	966.9951	1989.1605	Si25	460.0616	135.8942	Si25	519.6984	174.5462	C25	193.7582	127.3018
Si26	70.1612	70.1612	Si26	367.2007	441.4413	Si26	274.7445	749.6234	Si26	512.3460	205.8624
C27	44.7974	660.3342	C27	63.9877	576.2052	C27	119.1342	596.1158	Si27	330.7595	720.5845
C28	9184.2751	27936.5520	C28	951.7545	1628.9741	C28	100.1434	587.8998	C28	129.3061	602.9246
Si29	11614.9608	34892.0907	Si29	667.8744	1743.8550	Si29	124.7423	430.1404	C29	248.4134	359.0231
Si30	11034.4753	32697.5319	Si30	850.2937	2044.8832	Si30	131.5901	359.0858	Si30	783.4974	1414.9085
C31	3090.8008	5299.2386	C31	476.3385	756.2754	C31	142.2919	81.5811	Si31	658.5249	1384.6970
Si32	1802.3087	6359.0112	Si32	98.2057	701.4854	Si32	314.3669	272.1731	C32	110.2182	121.6634
			O33	235.2252	248.2998				Si33	558.9451	1001.1969

Isotropic chemical-shielding (σ_{iso}/ppm) & anisotropic chemical-shielding (σ_{aniso}/ppm): $\sigma_{iso} = \frac{\sigma 33 + \sigma 22 + \sigma 11}{3}$; $\sigma_{aniso} = \sigma 33 - \frac{\sigma 22 + \sigma 11}{2}$.

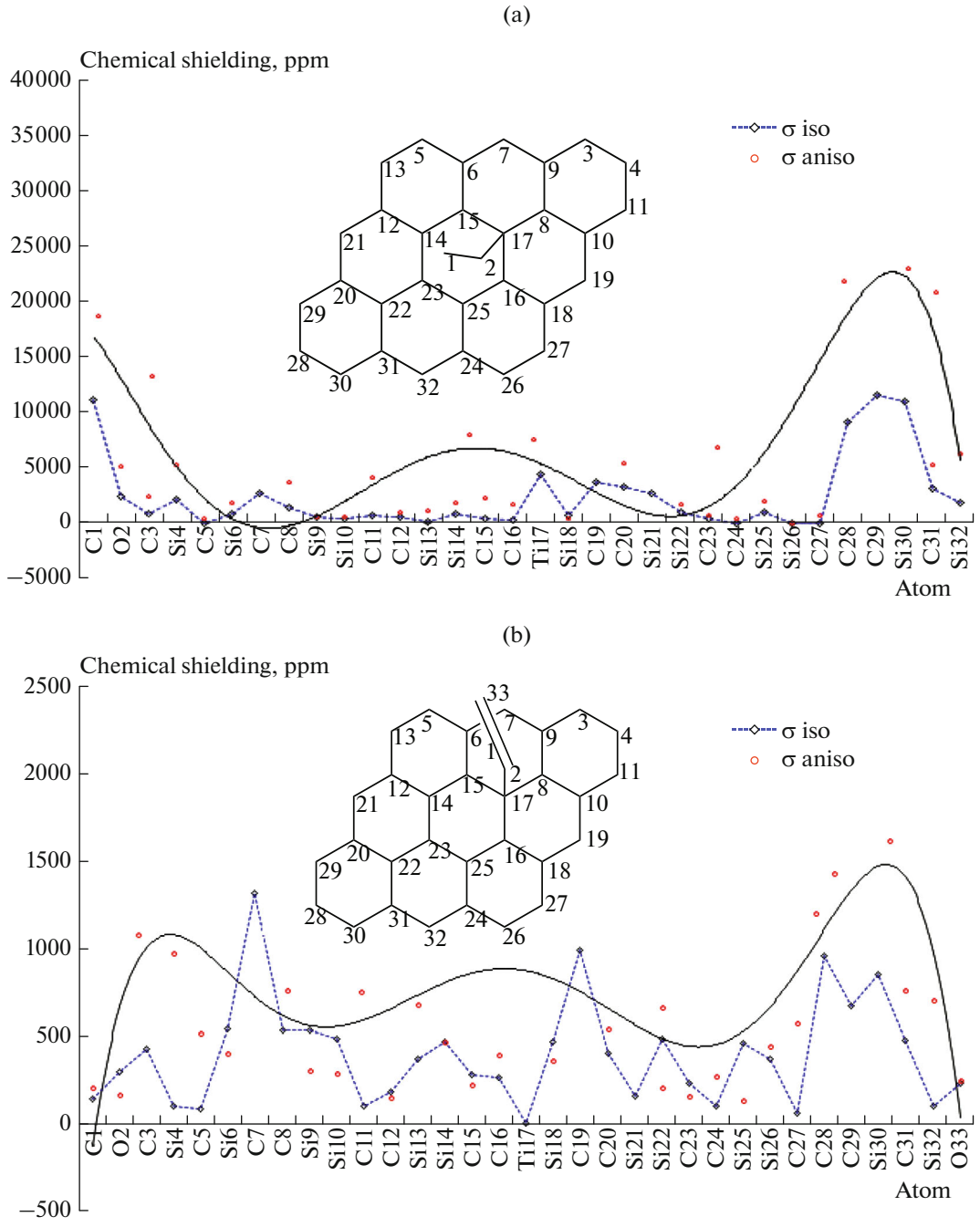

Fig. 5. NMR adsorbing of CO, CO_2, NO and NO_2 adsorbed on the Ti–SiC nanosheet through production of clusters of (a) CO@Ti–SiC_sh, (b) CO_2@Ti–SiC_sh, (c) NO@Ti–SiC_sh, and (d) NO_2@Ti–SiC_sh.

(Fig. 5c); and NO_2@Ti–SiC_sh with several sharp peaks for atoms of O3, Si14, Si22, Si27, Si30, Si31, and several less sharper peaks of N1, C6, Ti18 (Fig. 5d), respectively, have been indicated.

Although, in the NMR spectroscopy, it has been observed the remarkable peaks around silicon and titanium atoms in the SiC nanosheets through the adsorption procedure of gas molecules, there are some fluctuations in the chemical shielding behaviors of isotropic and anisotropy attributes.

In this section, the stability of complexes including gas adsorption on titanium (Ti) metal-doped graphene-like silicon carbide (SiC) monolayer sheet has been investigated through thermodynamic properties which define the reactions that CO, CO_2, NO, and NO_2 endure in the Ti–SiC_sh coordination sphere.

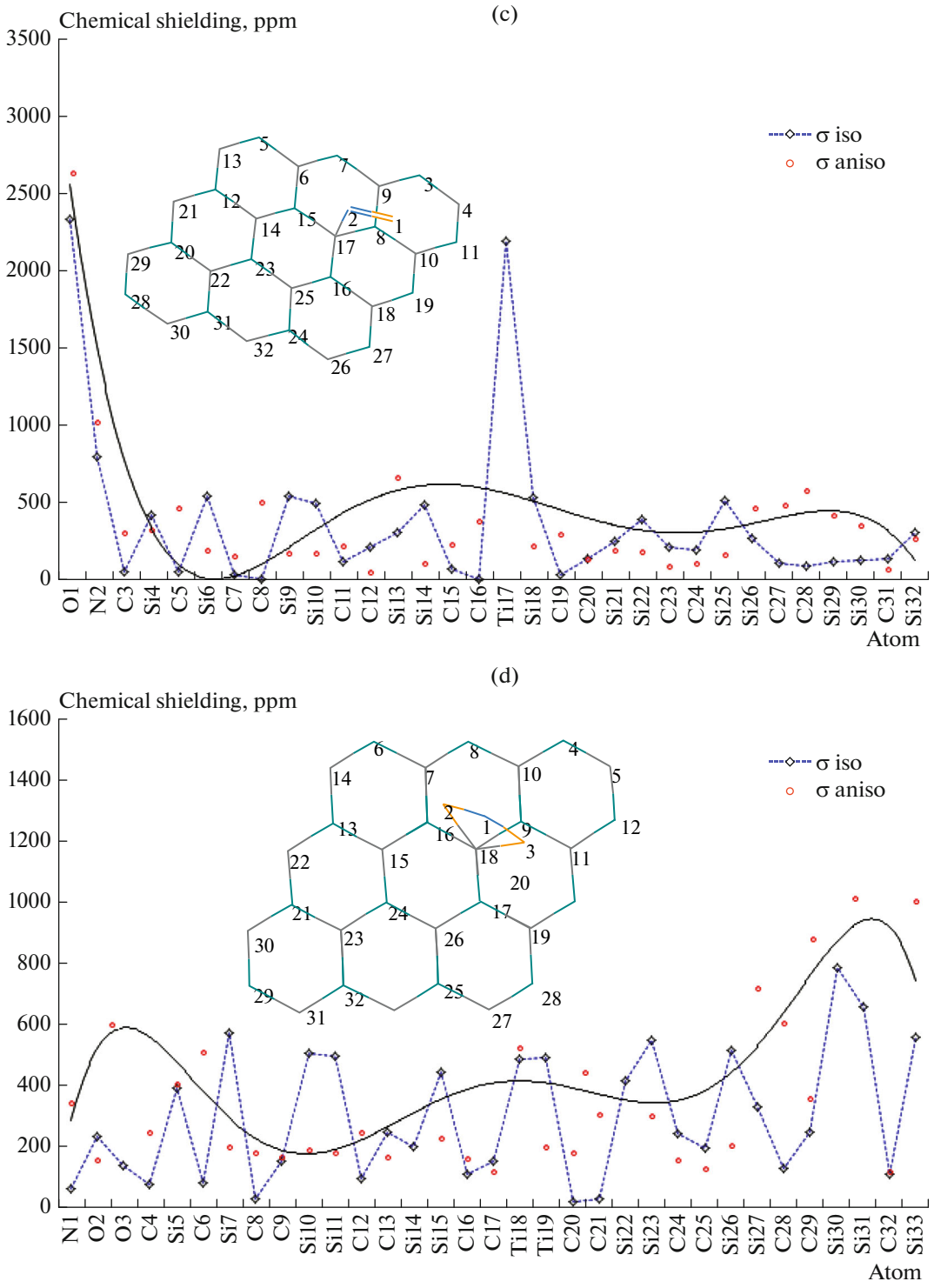

Fig. 5. (Contd.)

Concerning adsorption process, the thermodynamic characters were evaluated for CO, CO_2, NO, and NO_2 on the surface of Ti–SiC_sh as the gas detectors which can be applicable as the selective sensors for these gases (Table 3).

Based on Table 3, the orientations of the adsorbed gas molecules on the SiC surface exhibited a tendency to orient in the inclined and parallel forms to monolayer SiC_sh. The DFT analysis proposed that the monolayer SiC_sh with C and Ti-doped atoms having one satisfied

Table 3. The thermodynamic character of CO, CO_2, NO, and NO_2 adsorbed on the Ti–SiC_sh as the selective gas sensors

Compound	$\Delta E^\circ \times 10^{-4}$, kcal/mol	$\Delta H^\circ \times 10^{-4}$, kcal/mol	$\Delta G^\circ \times 10^{-4}$, kcal/mol	S°, cal/K mol	Dipole moment, Db
CO	−6.9784	−6.9784	−6.9798	47.100	0.2373
CO_2	−11.6121	−11.6121	−11.6136	51.378	0.0000
NO	−8.0017	−8.0016	−8.0031	48.968	0.2376
NO_2	−12.6298	−12.6298	−12.6315	57.792	0.2323
SiC_sh	−304.3389	−304.3389	−304.3417	93.684	9.6011
Ti–SiC_sh	−339.1002	−339.1001	−339.1029	93.419	10.1407
CO@Ti–SiC_sh	−346.1065	−346.1064	−346.1093	97.616	10.3155
CO_2@Ti–SiC_sh	−350.7642	−350.7642	−350.7671	100.038	10.0483
NO@Ti–SiC_sh	−347.1429	−347.1428	−347.1458	100.033	16.4330
NO_2@Ti–SiC_sh	−351.8006	−351.8006	−351.8036	102.455	16.1658

valency increased the Van der Waal interactions between the gas molecules and the monolayer SiC_sh. The overall analysis indicated that the adsorption strength of monolayer SiC_sh towards the chosen gas molecules follows the order: $NO_2 > CO_2 > NO > CO$.

Furthermore, the IR spectrums for adsorption of CO, CO_2, NO, and NO_2 on the surfaces of Ti–SiC_sh have been reported in Figs. 6a–6c. The graph of Fig. 6a has been observed in the frequency range between 500–2500 cm^{-1} for the complex of CO@Ti–SiC_sh with a sharp peak around 550 cm^{-1}.

Figure 6b has shown the several strongest IR peaks of CO_2@Ti–SiC_sh approximately between 1000–3000 cm^{-1} with a sharp peak of around 3000 cm^{-1}. Figure 6c has shown the several less stronger IR peaks of NO@Ti–SiC_sh approximately between 1500–2500 cm^{-1} with a sharp peak of around 1750 cm^{-1}. Moreover, Fig. 6d has denoted the several IR peaks of NO_2@Ti–SiC_sh approximately between 1000–2500 cm^{-1} with two sharp peaks around 1823.63 and 2039.31 cm^{-1}.

The adsorptive capacity of CO, CO_2, NO, and NO_2 on the surface of Ti–SiC_sh is approved by the ΔE°_{ads} amounts as formula:

$$\Delta E^\circ_{ads} = \Delta E^\circ_{X\to Ti-SiC\_sh} - \left(\Delta E^\circ_X + \Delta E^\circ_{Ti-SiC\_sh}\right), \quad (X = CO, CO_2, NO, NO_2). \quad (6)$$

Table 3 has shown that all the measured relative adsorption energies (ΔE°_{ads}) of CO, CO_2, NO, and NO_2 on the surface of Ti–SiC_sh are almost identical, and exhibit the accord of the estimated data by all methods and the accuracy of the calculations. In fact, Ti–SiC_sh has higher interaction energy from Van der Waals' forces with gas molecules including CO, CO_2, NO, and NO_2 that can make them highly stable.

Furthermore, the difference of ΔH_R among adsorption of CO, CO_2, NO, and NO_2 on the surface of Ti-doped SiC_sh has been unraveled due to non-covalent binding resulted from interatomic interactions between gas molecules and surface (GM@Ti–SiC) and covalent binding resulted from intra-atomic interactions between transition metal of titanium and silicon carbide nanosheet (Ti–SiC_sh) (Fig. 7).

Figure 7 has indicated the heat of formation (ΔH°_{ads}) between initial compounds of CO, CO_2, NO, NO_2, surface of SiC_sh, Ti-doped SiC_sh nanosheet and product compounds of CO@Ti–SiC_sh, CO_2@Ti–SiC_sh, NO@Ti–SiC_sh and NO_2@Ti–Si_sh with the polynomial curve of order = 3 and $R^2 = 0.8864$.

The amounts of ΔG°_{ads} versus dipole moment for CO, CO_2, NO, NO_2, Ti-doped SiC_sh surface, and complexes of CO@Ti-SiC_sh, CO_2@Ti-SiC_sh, NO@Ti-SiC_sh and NO_2@Ti-SiC_sh have been plotted in Fig. 8.

For the adsorption mechanism, ΔG°_{ads} is calculated as follows:

$$\Delta G^\circ_{ads} = \Delta G^\circ_{X\to Ti-SiC\_sh} - \left(\Delta G^\circ_X + \Delta G^\circ_{Ti-SiC\_sh}\right), \quad (X = CO, CO_2, NO, NO_2). \quad (7)$$

As shown in Table 3, all the computed ΔG°_{ads} amounts are close, which exhibits the accord of the evaluated data by all methods and the validity of the computations. However, Ti–SiC_sh surface seems possess enough efficiency for adsorption of gas molecules containing CO, CO_2, NO, and NO_2 through charge transfer from nitrogen and oxygen to the titanium element doping of silicon carbide due to intra-atomic and interatomic interactions.

In the case of adsorption, the area of the adsorbent becomes an additional thermodynamic variable. A similar situation arises for the equilibria of gas phase,

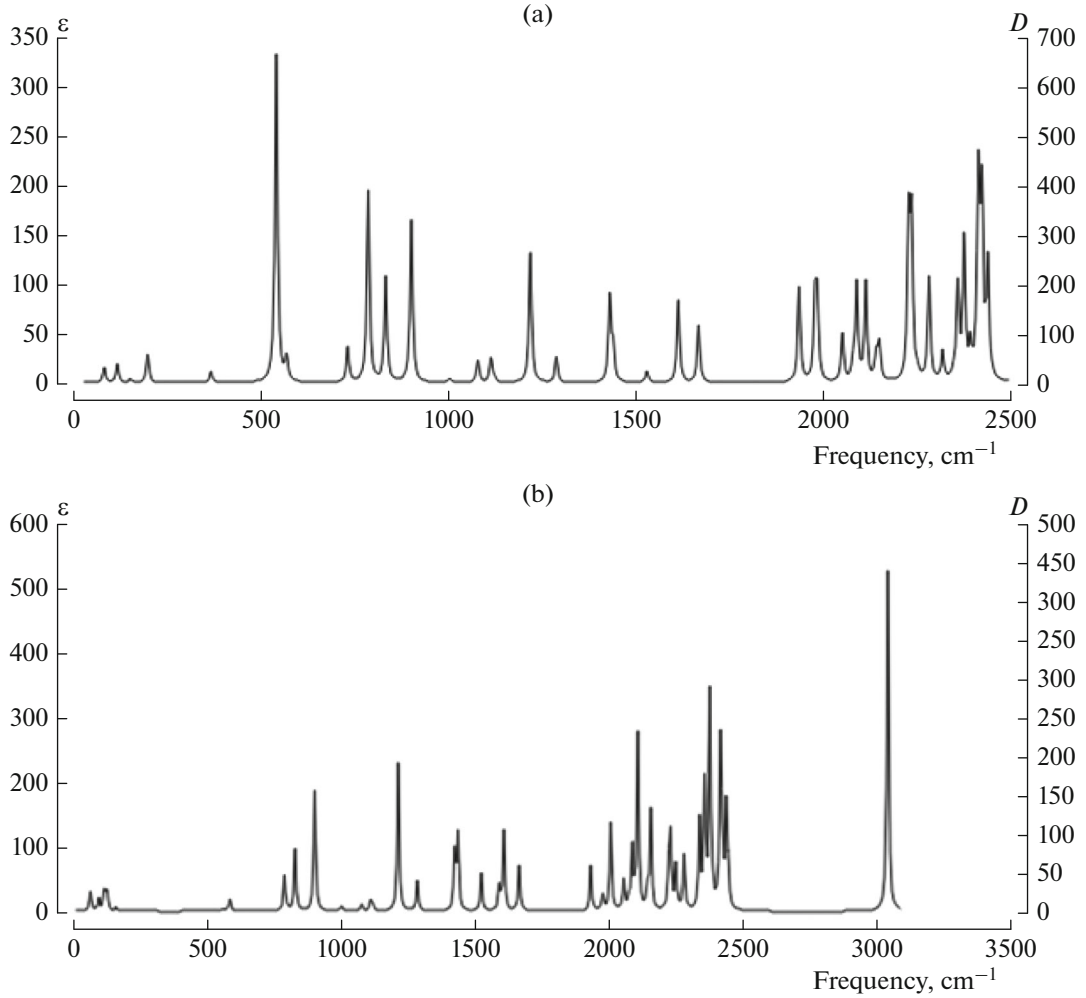

Fig. 6. The Frequency (cm^{-1}) changes through the "IR" spectrums for (a) CO@Ti–SiC_sh, (b) CO_2@Ti–SiC_sh, (c) NO@Ti–SiC_sh and (d) NO_2@Ti–SiC_sh as the selective gas detectors.

where a specification of gas molecule (CO, CO_2, NO, NO_2) is necessary to define the thermodynamic system. The pertinent additional intensive variable for the equilibria of gas molecule of CO, CO_2, NO, and NO_2 is surface tension; similarly, the spreading pressure becomes an additional intensive variable for adsorption equilibria (Table 3 and Figs. 7, 8).

From Fig. 8, ΔG°_{ads} may depend on the interactions between the gas molecules of CO, CO_2, NO, NO_2 and the Ti–SiC surface. In fact, comparison to ΔG°_{ads}, it is allocated a good accord ($R^2 = 0.9912$) among calculated results, and validity of the picked isotherm for the adsorption which produce the CO → Ti–SiC, CO_2 → Ti–SiC, NO → Ti–SiC and NO_2 → Ti–Si complexes.

In fact, SiC and Ti–SiC surfaces seem possess enough efficiency for adsorption toxic gases of CO, CO_2, NO, NO_2 through charge transfer from nitrogen and oxygen to silicon and the titanium atoms due to intra-atomic and interatomic interactions.

In other words, the adsorbent is assumed to be thermodynamically inert; that is the change in a thermodynamic property of the adsorbent, such as internal energy, during an adsorption process at constant temperature is assumed to be negligible compared with the change in the same property for the adsorbing gas.

Based on frontier molecular orbital (FMO) theory, the LUMO and HOMO and the energy between them is the band gap of the adsorption system were computed. In fact, broad band gap diagram indicates that there is less conductivity [54–56]. The LUMO, HOMO, band energy gap (ΔE) and other quantities distributions of CO, CO_2, NO, and NO_2 on the surfaces of Ti–SiC_sh as the gas detector systems denote that the gas adsorption procedure scatters the electrons of the system (Table 4) [55, 56].

The energy gap between HOMO and LUMO has represented the transporting of molecular electrical

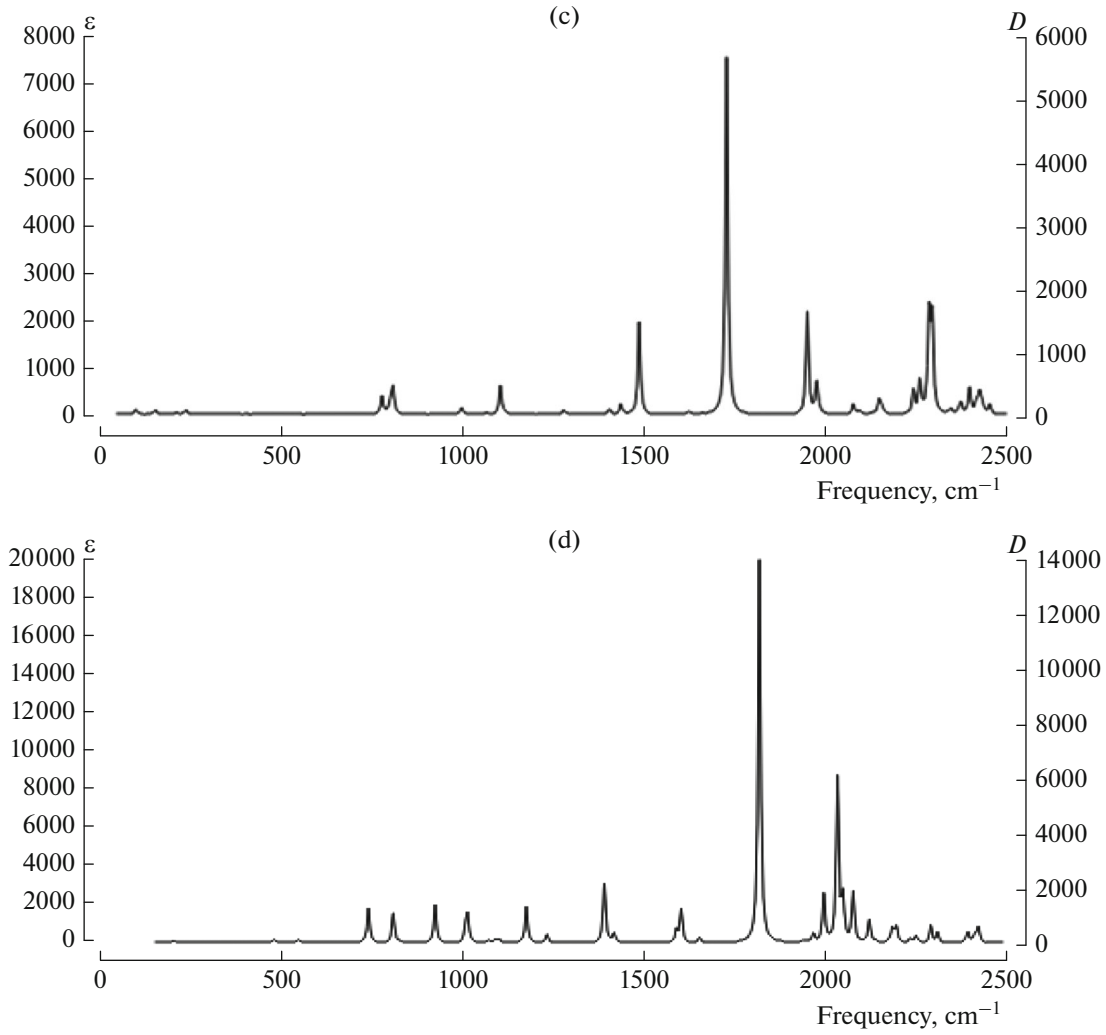

Fig. 6. (Contd.)

characters [57, 58]. On the other hand, the difference between HOMO and LUMO has exhibited that the effect of the adsorption process on the electronic behavior of CO, CO_2, NO, and NO_2 on the surfaces of Ti–SiC_sh nanosheet. Other quantities (eV) consisting of Chemical potential, electronegativity, hardness, Softness, and electrophilicity index show an agreeable yield for capturing CO, CO_2, NO, and NO_2 by Ti–SiC_sh nanosheet (Table 4).

The illustration of donor–acceptor molecules depends on the relative frontier molecular levels. The HOMO–LUMO gap defines the charge transfer in gas molecules adsorbed on the Ti–SiC_sh nanosheet through simplified molecular-level diagram. In fact,

Table 4. LUMO (eV), HOMO (eV), band energy gap (ΔE, eV) and other quantities (eV) distributions of CO, CO_2, NO, and NO_2 on the surfaces of Ti–SiC_sh

Gas → Ti–SiC_sh	HOMO	LUMO	ΔE	μ	χ	η	ζ	ψ
CO@Ti–SiC_sh	−0.2710	0.6038	0.8748	0.1664	−0.1664	0.4374	1.1431	0.0316
CO_2@Ti–SiC_sh	−0.0114	0.8560	0.8674	0.4223	−0.4223	0.4337	1.1528	0.2056
NO@Ti–SiC_sh	−1.1907	0.6011	1.7918	−0.2948	0.2948	0.8959	0.5581	0.0485
NO_2@Ti–SiC_sh	−1.4947	0.4933	1.988	−0.5007	0.5007	0.994	0.5030	0.1261

Band energy gap: $\Delta E = E_{LUMO} - E_{HOMO}$ (eV); chemical potential: $\mu = (E_{HOMO} + E_{LUMO})/2$ (eV); electronegativity: $\chi = -(E_{HOMO} + E_{LUMO})/2$ (eV); Hardness: $\eta = (E_{LUMO} - E_{HOMO})/2$ (eV); softness: $\zeta = 1/(2\eta)$ (eV); electrophilicity index: $\psi = \mu^2/(2\eta)$ (eV).

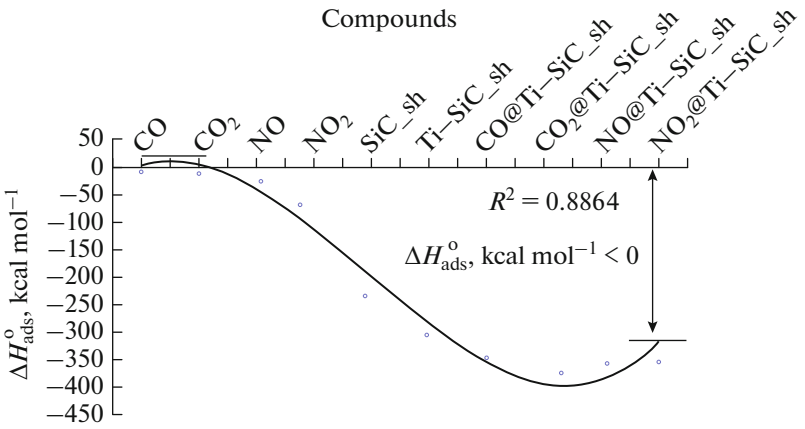

Fig. 7. The alterations of relative adsorption energy (ΔH°_{ads}/kcal mol^{-1}) for the reaction of CO, CO_2, NO, and NO_2 adsorbed on the surface of Ti–SiC_sh.

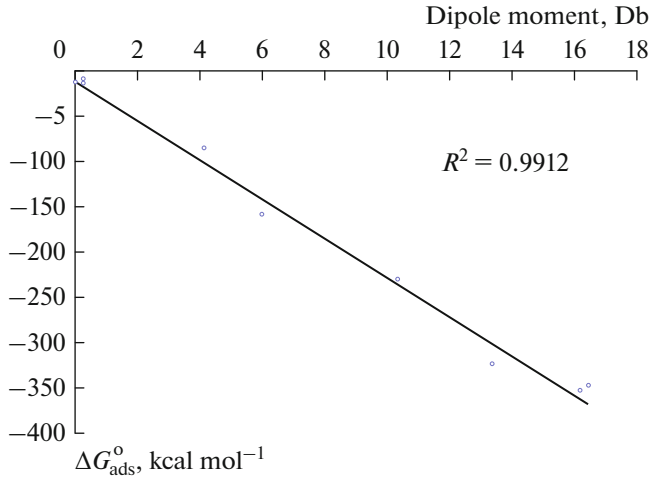

Fig. 8. Gibbs free energy (ΔG°_{ads}, kcal/mol) for adsorption of CO, CO_2, NO, and NO_2 on the surface of Ti–SiC_sh versus dipole moment (Debye).

the amount of transferred charges might be considerably small, as in the case of parallel and perpendicular coordination, which indicate electronic couplings smaller than in co-facial coordination [59–65]. The results in Table 4 have indicated the energy level shifts of gas molecule → surface-HOMO and gas molecule → surface-LUMO of nanoclusters as a function of their distance *d* orbitals from the high symmetry points of each gas molecule on the Ti–SiC_sh nanosheet. Therefore, the HOMO level of molecule is being lowered as it loses its electron, whereas the LUMO level of surface is being raised as it gains partial charge.

CONCLUSIONS

In summary, the nonmetal element-doped SiC nanosheet has been studied by first-principle calculations. Different dopants of gas molecules and doping sites are considered.

The current research wanted to remark the illustration of gas adsorption on Ti–SiC_sh nanosheet. Particularly, the structural, energetic, and infrared adsorption properties of linearly "atop" for CO, CO_2, NO, and NO_2 gas molecules adsorbing on Ti–SiC_sh nanosheet has been explored by using DFT calculations.

The values of changes of charge density have shown a more important charge transfer for Ti–SiC_sh nanosheet which acts as the electron acceptor while gas molecules act as the stronger electron donners through adsorption on the Ti–SiC_sh nanosheet surface. It has been assumed that the priority for selecting the surface binding of N-atom of NO, and O-atom of NO_2, CO and CO_2 in adsorption site can be impacted by the existence of close atoms in the Ti–SiC_sh surface.

In fact, Ti site in SiC_sh nanosheet has higher interaction energy from Van der Waals' forces with gas molecules including CO, CO_2, NO, and NO_2 that can make them highly stable. Finally, our molecular simulation consequences have exhibited the existence of orbital hybridization between titanium site and gas molecules of CO, CO_2, NO, and NO_2 that also approves the recovery of adsorption susceptibility of graphene sheet. In fact, Ti–SiC_sh surface can promise an applicable outlook in the field of CO, CO_2, NO, and NO_2 gas sensor.

Moreover, a thermodynamic formalism describing adsorption processes of gas molecules of CO, CO_2, NO, and NO_2 on the solid adsorbent of SiC and Ti–SiC surfaces has been developed. Besides, this process being treated as internal process of the adsorbent–adsorbate system. Thermodynamic parameters have constructed a detailed molecular model for atom–atom interactions and a distribution of point charges is used to reproduce the polarity of the solid material and the adsorbing molecules [66–69].

ACKNOWLEDGMENTS

In successfully completing this paper and its research, the authors are grateful to Kastamonu University for their support through the office, library, and scientific websites.

FUNDING

This work was supported by ongoing institutional funding. No additional grants to carry out or direct this particular research were obtained.

CONFLICT OF INTEREST

The authors of this work declare that they have no conflicts of interest.

REFERENCES

1. J. Zhang, W. Wang, Russ. J. Phys. Chem. B **17**, 293 (2023). https://doi.org/10.1134/S1990793123020343
2. F. Mollaamin, M. Monajjemi, J. Bio- Tribo-Corros. **9**, 47 (2023). https://doi.org/10.1007/s40735-023-00768-3
3. M. M. Avilova, N. V. Zolotareva, and O. V. Popova, Russ. J. Phys. Chem. B **17**, 329 (2023). https://doi.org/10.1134/S1990793123020203
4. A. H. Davtyan, Z. O. Manukyan, S. D. Arsentev, et al., Russ. J. Phys. Chem. B **17**, 336 (2023). https://doi.org/10.1134/S1990793123020239
5. F. Mollaamin and M. Monajjemi, J. Cluster Sci. **34** (6), 1–18 (2023). https://doi.org/10.1007/s10876-023-02436-5
6. O. N. Fedyaeva, A. V. Shishkin, and A. A. Vostrikov, Russ. J. Phys. Chem. B **16**, 1285 (2022). https://doi.org/10.1134/S1990793122070053
7. F. Mollaamin and M. Monajjemi, Mol. Simul. **49** (4), 365 (2023). https://doi.org/10.1080/08927022.2022.2159996
8. M. Monajjemi, M. T. Baie, and F. Mollaamin, Russ. Chem. Bull. **59**, 886 (2010). https://doi.org/10.1007/s11172-010-0181-5
9. K. Bakhshi, F. Mollaamin, M. Monajjemi, J. Comput. Theor. Nanosci. **8**, 763 (2011). https://doi.org/10.1166/jctn.2011.1750
10. G. M. Khrapkovskii, I. V. Aristov, D. L. Egorov, et al., Russ. J. Phys. Chem. B **16**, 862–868 (2022). https://doi.org/10.1134/S1990793122040066
11. M. Khaleghian, M. Zahmatkesh, F. Mollaamin, and M. Monajjemi, Fullerenes, Nanotubes and Carbon Nanostructures **19**, 251 (2011). https://doi.org/10.1080/15363831003721757
12. F. Mollaamin, M. Monajjemi, J. Mol. Model. **29**, 170 (2023). https://doi.org/10.1007/s00894-023-05567-8
13. B. P. Aduev, D. R. Nurmukhametov, N. V. Nelyubina, et al., Russ. J. Phys. Chem. B **17**, 361 (2023). https://doi.org/10.1134/S1990793123020033
14. F. Mollaamin and M. Monajjemi, Sensor Rev. **43** (37) 1–14 (2023). https://doi.org/10.1108/SR-03-2023-0040
15. N. V. Dokhlikova, A. K. Gatin, S. Y. Sarvadiy, et al., Russ. J. Phys. Chem. B **16**, 772 (2022). https://doi.org/10.1134/S1990793122040042
16. F. Mollaamin and M. Monajjemi, C **9**, 20 (2023). doi
17. S. K. Dolukhanyan, A. G. Aleksanyan, O. P. Ter-Galstyan, et al., Russ. J. Phys. Chem. B **16**, 76 (2022). https://doi.org/10.1134/S1990793122010043
18. F. Mollaamin and M. Monajjemi, Clean Technol. **5** (1), 403–417 (2023). https://doi.org/10.3390/cleantechnol5010020
19. F. Mollaamin and M. Monajjemi, J. Mol. Model. **29**, 119 (2023). https://doi.org/10.1007/s00894-023-05526-3
20. X. Miao, S. Zhou, and C. Wang, Russ. J. Phys. Chem. B **16**, 804 (2022). https://doi.org/10.1134/S199079312204011X
21. M. V. Grishin, A. K. Gatin, V. G. Slutskii, et al., Russ. J. Phys. Chem. B **16**, 395 (2022). https://doi.org/10.1134/S1990793122030150
22. H. Ou, X. Shi, Y. Lu, et al., Mater. **16**, 1014 (2023). https://doi.org/10.3390/ma16031014
23. N. V. Dokhlikova, A. K. Gatin, S. Y. Sarvadiy, et al., Russ. J. Phys. Chem. B **16**, 361 (2022). https://doi.org/10.1134/S1990793122020166
24. S. Zhu, T. Liu, J. Fan, et al., Mater. **15**, 5995 (2022). https://doi.org/10.3390/ma15175995
25. S. Das, Y. Zheng, A. Ahyi, et al., Mater. **15**, 6736 (2022). https://doi.org/10.3390/ma15196736
26. N. A. Kochetov, B. S. Seplyarsky, Russ. J. Phys. Chem. B **16**, 66 (2022). https://doi.org/10.1134/S1990793122010079
27. A. A. Dyshin, M. S. Kuzmikov, A. A. Aleshonkova, et al., Russ. J. Phys. Chem. B **15**, 1221 (2021). https://doi.org/10.1134/S1990793121080030

28. F. La Via, D. Alquier, F. Giannazzo, et al., Micromachines **14** (6), 1200 (2023). https://doi.org/10.3390/mi14061200
29. S. Wang and M. Li, Russ. J. Phys. Chem. B **15** (Suppl. 2), S181 (2021). https://doi.org/10.1134/S1990793121100079
30. S. Oglesby and S. A. Ivanov, A. Londonõ-Calderon, et al., Matererials **15**, 3475 (2022). https://doi.org/10.3390/ma15103475
31. F. Mollaamin and M. Monajjemi, Computation **11**, 108 (2023). https://doi.org/10.3390/computation11060108
32. L. S. Shibryaeva, L. R. Lyusova, S. G. Karpova, et al., Russ. J. Phys. Chem. B **16**, 334 (2022). https://doi.org/10.1134/S199079312202021X
33. E. V. Ramos-Fernández and J. Narciso, Materials **16**, 2034 (2023). https://doi.org/10.3390/ma16052034
34. S. Shikunov, A. Kaledin, I. Shikunova, et al., Coatings **13**, 354 (2023). https://doi.org/10.3390/coatings13020354
35. M. I. Skobin, M. A. Feofanova, V. M. Nikolskiy, et al., Russ. J. Phys. Chem. B **16**, 329 (2022). https://doi.org/10.1134/S1990793122020245
36. J. P. Perdew, K. Burke, and M. Ernzerhof, "Generalized gradient approximation made simple," Phys. Rev. Lett. **77**, 3865 (1996). https://doi.org/10.1103/PhysRevLett.77.3865
37. I. L. Fufurin, I. B. Vintaikin, A. L. Nazolin, et al., Russ. J. Phys. Chem. B **16**, 483 (2022). https://doi.org/10.1134/S1990793122030034
38. A. Kaledin, S. Shikunov, K. Komarov, et al., Metals **13**, 313 (2023). https://doi.org/10.3390/met13020313
39. F. Mollaamin, S. Shahriari, M. Monajjemi, et al., J. Cluster Sci. **34**, 1547 (2023). https://doi.org/10.1007/s10876-022-02335-1
40. M. Monajjemi, F. Mollaamin, M.R. Gholami, et al., Main Group Met. Chem. **26**, 349 (2003). https://doi.org/10.1515/MGMC.2003.26.6.349
41. R. Dennington, T. A. Keith, J. M. Millam, GaussView. Version 6 (Shawnee Mission, KS, Semichem Inc., 2016).
42. M. J. Frisch, G. W. Trucks, H. B. Schlegel, G. E. Scuseria, M. A. Robb, J. R. Cheeseman, G. Scalmani, V. Barone, G. A. Petersson, H. Nakatsuji, X. Li, M. Caricato, A. V. Marenich, J. Bloino, B. G. Janesko, R. Gomperts, B. Mennucci, H. P. Hratchian, J. V. Ortiz, A. F. Izmaylov, J. L. Sonnenberg, D. Williams-Young, F. Ding, F. Lipparini, F. Egidi, J. Goings, B. Peng, A. Petrone, T. Henderson, D. Ranasinghe, V. G. Zakrzewski, J. Gao, N. Rega, G. Zheng, W. Liang, M. Hada, M. Ehara, K. Toyota, R. Fukuda, J. Hasegawa, M. Ishida, T. Nakajima, Y. Honda, O. Kitao, H. Nakai, T. Vreven, K. Throssell, J. A. Montgomery, Jr., J. E. Peralta, F. Ogliaro, M. J. Bearpark, J. J. Heyd, E. N. Brothers, K. N. Kudin, V. N. Staroverov, T. A. Keith, R. Kobayashi, J. Normand, K. Raghavachari, A. P. Rendell, J. C. Burant, S. S. Iyengar, J. Tomasi, M. Cossi, J. M. Millam, M. Klene, C. Adamo, R. Cammi, J. W. Ochterski, R. L. Martin, K. Morokuma, O. Farkas, J. B. Foresman, and D. J. Fox, Gaussian 16, Revision C.01 (Gaussian, Inc., Wallingford CT, 2016).
43. I. A. Shtepliuk, Sensors **23**, 5631 (2023). https://doi.org/10.3390/s23125631
44. F. Mollaamin, M. Monajjemi, S. Salemi, et al., Fullerenes, Nanotubes and Carbon Nanostructures **19** (3), 182 (2011). https://doi.org/10.1080/15363831003782932
45. S. Lehtola, Int. J. Quantum Chem. **119** (19), e25968 (2019). https://doi.org/10.1002/qua.25968
46. A. K. Gatin, M. V. Grishin, A. S. Prostnev, et al., Russ. J. Phys. Chem. B **16**, 468 (2022). https://doi.org/10.1134/S1990793122030046
47. A. S. Tarasov, V. A. Golyashov, I. O. Akhundov, et al., Russ. J. Phys. Chem. B **16**, 479 (2022). https://doi.org/10.1134/S1990793122030241
48. N. V. Dokhlikova, S. A. Ozerin, S. V. Doronin, et al., Russ. J. Phys. Chem. B **16**, 461 (2022). https://doi.org/10.1134/S1990793122030137
49. V. G. Kytin, A. V. Duvakina, E. A. Konstantinova, et al., Russ. J. Phys. Chem. B **16**, 421 (2022). https://doi.org/10.1134/S1990793122030186
50. E. M. Lozben, A. V. Lebedev, M. A. Deminsky, et al., Russ. J. Phys. Chem. B **16**, 381 (2022). https://doi.org/10.1134/S1990793122030095
51. F. Mollaamin, M. Monajjemi, J. Comput. Theor. Nanosci. **12** (6), 1030 (2015). https://doi.org/10.1166/jctn.2015.3846
52. M. Monajjemi, H. Baheri, F. Mollaamin, J. Struct. Chem. **52**, 54 (2011). https://doi.org/10.1134/S0022476611010070
53. S. O. Adamson, D. D. Kharlampidi, G. V. Golubkov, et al., Russ. J. Phys. Chem. B **15**, 755 (2021). https://doi.org/10.1134/S1990793121050122
54. M. Monajjemi, N. Farahani, and F. Mollaamin, Phys. Chem. Liq. **50**, 161 (2012). https://doi.org/10.1080/00319104.2010.527842
55. M. A. A. Zadeh, H. Lari, L. Kharghanian, et al., J. Comput. Theor. Nanosci. **12**, 4358 (2015). https://doi.org/10.1166/jctn.2015.4366
56. B. Ghalandari, M. Monajjemi, F. Mollaamin, J. Comput. Theor. Nanosci. **8**, 1212 (2011). https://doi.org/10.1166/jctn.2011.1801
57. M. Monajjemi, L. Mahdavian, F. Mollaamin, et al., Russ. J. Inorganic Chem. **54**, 1465 (2009). https://doi.org/10.1134/S0036023609090216
58. S. Sarvendra Kumar, and M. K. Yadav, Russ. J. Phys. Chem. B **15** (Suppl 1), S22 (2021). https://doi.org/10.1134/S1990793121090116
59. B. Khalili Hadad, F. Mollaamin, and M. Monajjemi, Russ. Chem. Bull. **60**, 238 (2011). https://doi.org/10.1007/s11172-011-0039-5
60. M. Monajjemi, F. Mollaamin, and S. Shojaei, Biointerface Res. Appl. Chem. **3**, 5575 (2020). https://doi.org/10.33263/BRIAC103.575585
61. A. Tahan, F. Mollaamin, and M. Monajjemi, Russ. J. Phys. Chem. A **83**, 587 (2009). https://doi.org/10.1134/S003602440904013X

62. M. Monajjemi, M. Khaleghian, N. Tadayonpour, et al., Int. J. Nanosci. **9** (5), 517–529 (2010). https://doi.org/10.1142/S0219581X10007071

63. F. Mollaamin and M. Monajjemi, Russ. J. Phys. Chem. B **17**, 658–672 (2023). https://doi.org/10.1134/S1990793123030223

64. F. Mollaamin, A. Ilkhani, N. Sakhaei, et al., J. Comput. Theor. Nanosci. **12**, 3148 (2015). https://doi.org/10.1166/jctn.2015.4092

65. E. M. Sarasia, S. Afsharnezhad, B. Honarparvar, et al., Phys. Chem. Liq. **49**, 561 (2011). https://doi.org/10.1080/00319101003698992

66. A. A. Lundin and V. E. Zobov, Russ. J. Phys. Chem. B **15**, 839 (2021). https://doi.org/10.1134/S1990793121050079

67. F. Mollaamin and M. Monajjemi, **C9**, 20 (2023). doi

68. V. F. Kablov, V. L. Strakhov, V. O. Kaledin, et al., Russ. J. Phys. Chem. B **15**, 880 (2021). https://doi.org/10.1134/S1990793121050043

69. A. Ghaffar, S. Nawaz, A. Munawar, et al., Russ. J. Phys. Chem. B **15** (Suppl 1), S42 (2021). https://doi.org/10.1134/S1990793121090074